Chemical Vapor Deposition

DOI: 10.1002/cvde.201307054

Full Paper

Atomic Layer Deposition of W:Al_2O_3 Nanocomposite Films with Tunable Resistivity**

By *Anil U. Mane* and *Jeffrey W. Elam**

Nanocomposite tungsten-aluminum oxide (W:Al_2O_3) thin films were prepared by atomic layer deposition (ALD) using tungsten hexafluoride (WF_6) and disilane (Si_2H_6) for the W ALD and trimethyl aluminum (TMA) and H_2O for the Al_2O_3 ALD. Quartz crystal microbalance (QCM) measurements performed using various W cycle percentages revealed that the W ALD inhibits the Al_2O_3 ALD and vice versa. Despite this inhibition, the relationship between W content and W cycle percentage was close to that predicted by theoretical calculations based on the growth per cycle values of binary compounds. Depth profiling XPS showed that the (W:Al_2O_3) films were uniform in composition and contained Al, O, and metallic W as expected, but also included significant F and C. Cross-sectional TEM revealed the composite film structure to be metallic nanoparticles (~1 nm) embedded in an amorphous matrix. The resistivity of these composite films could be tuned in the range of 10^{12}–10^{8} Ω cm by adjusting the W cycle percentage between 10% and 30%W. These films have applications in electron multipliers as well as electron and ion optics.

Keywords: ALD, Al_2O_3, Nanocomposites, Resistive coatings, Tungsten

1. Introduction

Thin film materials comprised of blended conducting and insulating components have been utilized in a wide variety of applications including resistive layers for electron multipliers such as microchannel plates,[1–3] resistive memories,[4–8] electro-chromic devices,[9–15] biomedical devices,[16–18] and charge-dissipating coatings on micro-electromechanical systems (MEMS) devices.[19–23] The physical and electrical properties of composite thin films can be tailored by adjusting the relative proportions of the constituent materials. Amongst the various thin-film deposition processes, atomic layer deposition (ALD) is a technique for growing complex layers in a precisely controlled manner with many unique advantages.[24] ALD is based on a binary sequence of self-limiting chemical reactions between precursor vapors and a solid surface. Because the two reactions in the binary sequence are performed separately, the gas phase precursors are never mixed and this eliminates the possibility of gas phase reactions that can form particulate contaminants and cause non-self-limiting chemical vapor deposition. This strategy yields monolayer-level thickness and composition control. The self-limiting aspect of ALD leads to continuous pinhole-free films, excellent step coverage, and conformal deposition on very high aspect ratio structures. ALD processing is also extendible to large area substrates and batch processing of multiple substrates.[24]

In this study, we synthesized composite thin films by combining the ALD processes for tungsten (W)[25] and aluminum oxide (Al_2O_3).[26] The ALD of W:Al_2O_3 nanolaminates composed of alternating distinct layers of these two materials has been explored previously, and these nanolaminates have been utilized as thermal barrier coatings and X-ray reflection coatings.[27–29] In contrast to this previous work, our study focused on synthesizing more thoroughly mixed W:Al_2O_3 composites in an effort to achieve unique electrical properties distinct from either material in their bulk forms. This approach has been employed previously for the ALD of metal oxide composite materials including ZnO-Al_2O_3[30,31] and Nb_2O_5-Ta_2O_5,[32,33] but to our knowledge this manuscript describes the first study of precisely controlled metal-metal oxide nanocomposites by ALD.

The motivation for our work is to develop tunable resistive coatings by ALD for application in microchannel plate (MCP) electron multipliers in large-area photodetectors.[34] We selected the W:Al_2O_3 system for a number of reasons. ALD W has a very low electrical resistivity of $\rho \sim 10^{-4}$ Ω cm[25] while ALD Al_2O_3 is an excellent insulator with a resistivity of $\rho \sim 10^{16}$ Ω cm.[35] This contrast offers the potential for an extremely wide range of tunable resistance values. In addition, ALD Al_2O_3 has a high breakdown electric field[35] and this attribute is beneficial in high voltage

[*] Dr. A. U. Mane, Dr. J. W. Elam
Energy Systems Division, Argonne National Laboratory, Argonne, IL 60439 (USA)
E-mail: jelam@anl.gov

[**] This work was supported by the U. S. Department of Energy, Office of Science, Office of Basic Energy Sciences and Office of High Energy Physics under contract DE-AC02-06CH11357 as part of the Large Area Picosecond Photodetector (LAPPD) project.

operating devices such as MCPs where the electric fields can exceed $10^6\,V\,m^{-1}$. Both W and Al_2O_3 ALD are performed under similar process conditions including the deposition temperature, and this simplifies the task of combining these materials into composite layers. In addition to the wide variance in electrical properties, W and Al_2O_3 have very different physical and chemical properties. As a result, by modulating the proportion of W in the Al_2O_3 matrix, we expect that the optical, mechanical, and electrical properties of W:Al_2O_3 composite layers can be broadly adjusted. Finally, both Al_2O_3 and W ALD are well-established processes used in semiconductor manufacturing and this bodes well for the eventual scale-up of W:Al_2O_3 composite layers.

Al_2O_3 ALD can be accomplished using alternating exposures to trimethyl aluminum (TMA) and H_2O.[26] W ALD can be performed using alternating exposures to Si_2H_6 and WF_6.[25] The surface chemistries for the individual half-reactions of the W and Al_2O_3 ALD have been examined in great detail.[36–38] In contrast, the surface chemistry for W:Al_2O_3 composite ALD is largely unexplored and is likely complex due to unique reactions that occur during the frequent transitions between the two materials. It is well known that Al_2O_3 ALD is mediated by surface hydroxyl (OH) groups,[26] while W ALD occurs via the sacrificial exchange of Si by W where the surface is partially F-terminated after both half-reactions.[25] In contrast, the reaction of TMA with surface F species is unknown, but a recent publication demonstrated that alternating exposures to niobium pentafluoride and TMA yielded films composed of niobium carbide, niobium fluoride, aluminum fluoride, and amorphous carbon.[39] Similarly, the reactions of Si_2H_6 and WF_6 are modulated by the OH-terminated alumina such that the ALD W growth per cycle is suppressed for ~10 cycles.[37,40]

This study explored the ALD synthesis of W:Al_2O_3 composite films to evaluate the effect of the ALD process parameters on the growth, composition, and properties of the resulting films. We employ in situ quartz crystal microbalance (QCM) measurements to perform a phenomenological study of the growth behavior of these films.

2. Results and Discussion

2.1. QCM Studies

In-situ QCM measurements were performed to examine the influence of the W cycle ratio on the growth of the W:Al_2O_3 composite layers. We define the W cycle ratio as: $\%W = W/(W + Al_2O_3)100$, where W and Al_2O_3 are the relative numbers of TMA/H_2O and Si_2H_6/WF_6 cycles performed, respectively. Figure 1a shows the mass changes registered for each ALD cycle during the growth of W:Al_2O_3 using 4 Al_2O_3 cycles between each W cycle, or 20% W cycles. The solid circles indicate the Al_2O_3 ALD cycles and the open circles represent the W ALD cycles. The dashed, horizontal line at $35\,ng\,cm^{-2}$ indicates the QCM step size observed during pure Al_2O_3 ALD. For reference, the QCM step size observed for pure W ALD is $930\,ng\,cm^{-2}$, which is off-scale in Fig. 1a. The first Al_2O_3 ALD cycle immediately following each W cycle is substantially diminished to an average value of $10\,ng\,cm^{-2}$. The Al_2O_3 growth then increases towards the nominal $35\,ng\,cm^{-2}$ value during the subsequent Al_2O_3 ALD cycles. Similarly, the W step size following the 4 ALD Al_2O_3 cycles is only $170\,ng\,cm^{-2}$, significantly below the steady-state value of $930\,ng\,cm^{-2}$ for pure W ALD.

Figure 1b shows the in-situ QCM data recorded during the W:Al_2O_3 ALD with 50% W cycles using the same vertical axis scale as Fig. 1a. The results are similar to the 20% W data in that both the Al_2O_3 and W growth are reduced compared to their steady-state values. Finally, Fig. 1c shows the QCM step size measurements recorded using 80% W cycles. The solid horizontal line indicates the QCM step size observed for pure W ALD, $930\,ng\,cm^{-2}$. Note that the vertical scale in Fig. 1c is ~4 times larger than in Fig. 1a,b. As before, the W ALD is inhibited following the

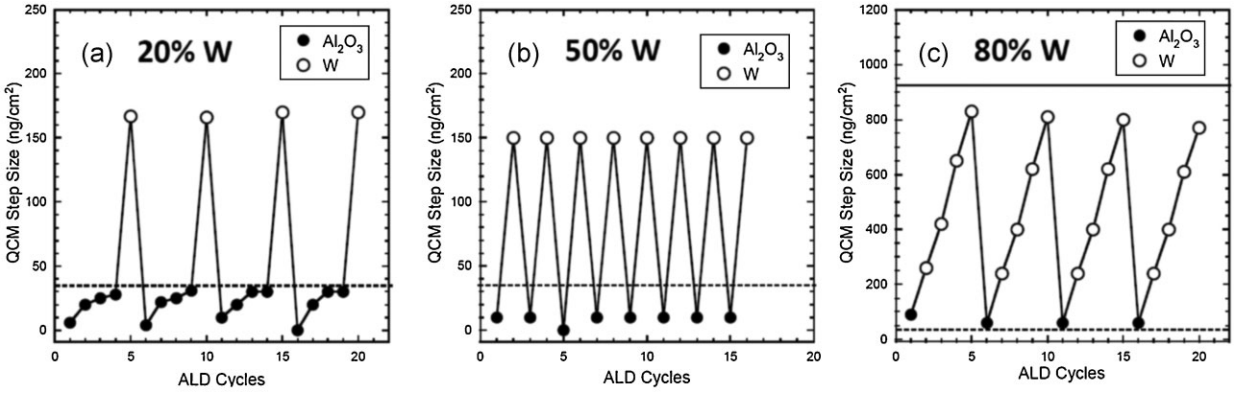

Fig. 1. In situ QCM measurements performed during the ALD of W:Al_2O_3 composite films using W cycle ratios of a) 20%, b) 50%, and c) 80%. The solid circles show the mass changes resulting from the individual Al_2O_3 ALD cycles, while the open circles show the mass changes from the W ALD cycles. The dashed line at $35\,ng\,cm^{-2}$ and solid line at $930\,ng\,cm^{-2}$ indicate the steady-state mass per cycle values for pure Al_2O_3 and W ALD, respectively.

single Al_2O_3 ALD cycle, but increases steadily and approaches the steady-state value during the subsequent W ALD cycles. It is interesting to note that the single Al_2O_3 ALD cycles in Fig. 1c deposit a greater mass than the nominal 35 ng cm^{-2} value suggesting enhanced growth.

Figure 2 summarizes the in-situ QCM measurements performed for the W:Al_2O_3 composite films. The solid circles plot the average Al_2O_3 step size and the open circles show the average W step size. The open triangles in the upper graph plot the relative W content for the composite films as determined by X-ray fluorescence (XRF) measurements of films deposited on Si substrates. As before, the dashed line at 35 ng cm^{-2} and solid line at 930 ng cm^{-2} indicate the steady-state mass per cycle values for the Al_2O_3 and W ALD, respectively. Below 50% W cycles, the average Al_2O_3 step size increases with decreasing %W. This behavior is expected because the average Al_2O_3 step size is smallest at 50% W where a single, inhibited Al_2O_3 ALD cycle is performed, but increases for multiple, successive Al_2O_3 ALD cycles as the Al_2O_3 ALD approaches the steady state. The same explanation describes the increase in average W step size above 50% W. The fact that the average W step size remains nearly constant below 50% W suggests that the initial reactions of Si_2H_6 and WF_6 are independent of the Al_2O_3 coverage or thickness. In contrast, the average Al_2O_3 step size increases above 50% W to values exceeding 2 times the steady-state ALD Al_2O_3 growth per cycle, suggesting that the TMA and H_2O reactions are somehow promoted on the thicker or more continuous W films. As we describe below, we believe these differences relate to AlF_3 formation on the F-terminated W surfaces. The general behavior of the W XRF signal is similar to the corresponding W QCM measurements, but the XRF signals are somewhat lower, especially near the 50% W region.

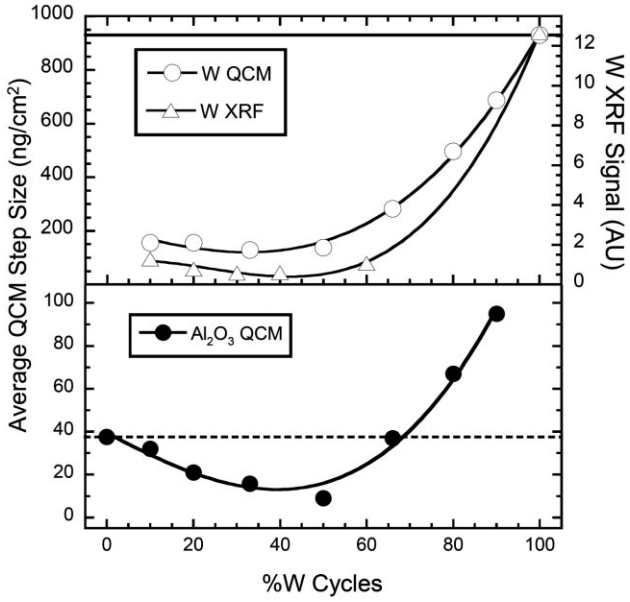

Fig. 2. Summary of in situ QCM measurements performed during the ALD of W:Al_2O_3 composite films. Left axis plots the average QCM step size from the Al_2O_3 (solid circles) and W (open circles) ALD cycles. Right axis plots the relative W XRF signals measured from W:Al_2O_3 composite films deposited on Si substrates (open triangles). The solid and dashed horizontal lines indicate the steady-state mass per cycle values for pure Al_2O_3 and W ALD, respectively, and the solid curves through the data points are intended to guide the eye.

The composition of the W:Al_2O_3 composite films can be estimated from the QCM measurements if one assumes that the mass deposited by the TMA/H_2O and Si_2H_6/WF_6 cycles correspond to pure Al_2O_3 and W, respectively. Assuming densities of 3.5[43] and 16.7[44] g cm^{-3} for the Al_2O_3 and W, respectively, Figure 3a plots the composition expressed as: mol W/(mol W + mol Al_2O_3)*100% versus the W cycle ratio. The solid line in Fig. 3a shows the rule-of-mixtures composition that would result if both materials were deposited at their steady-state values (i.e., no inhibition or promotion upon transitioning between materials).[30,31] The dashed line through the experimental data is intended to guide the eye. The compositions extracted from the QCM measurements are fairly similar to the rule-of-mixture values. Evidently the W and Al_2O_3 inhibition partially cancel so that the composition, which depends on the ratio, is not severely perturbed.

The W:Al_2O_3 composite film growth per cycle can also be extracted from the QCM measurements assuming the bulk densities listed above, and these results are shown as the solid circles in Fig. 3b. For comparison, the open circles in Fig. 3b show the growth per cycle measurements obtained by ellipsometry for the ALD W:Al_2O_3 composite films deposited on Si substrates. For both sets of measurements, the dashed lines guide the eye. The 5 Å per cycle W growth rate in Fig. 3b is unusually high for an ALD process, and is believed to result from >1 ML of Si deposited during the Si_2H_6 exposures, perhaps through silylene insertion into Si-H bonds, followed by the 1:1 replacement of Si by W during the following WF_6 exposure.[29,36,37,40]

The solid line in Fig. 3b shows the rule-of-mixtures values for the growth per cycle. As expected based on the mutual inhibition behavior seen in QCM, the growth per cycle values determined by both QCM and ellipsometry are significantly below the rule-of-mixtures values, and this deviation is greatest at 50% where the transitions between W and Al_2O_3 ALD cycles occur most frequently. It is somewhat surprising, however, that the QCM measurements are lower than the corresponding ellipsometry measurements in Fig. 3b. One explanation for this discrepancy is that the material deposited during the transitions between W and Al_2O_3 ALD has a lower density than expected. In agreement with this idea, X-ray photoelectron spectroscopy (XPS) measurements (Section 2.2) reveal that the ALD W:Al_2O_3 composite films contain AlF_3, and this material has a much lower density of 2.88 g cm^{-3} compared to W (16.7 g cm^{-3}).

The first TMA/H_2O cycle following the W ALD in the W:Al_2O_3 composite growth produces only a very small mass

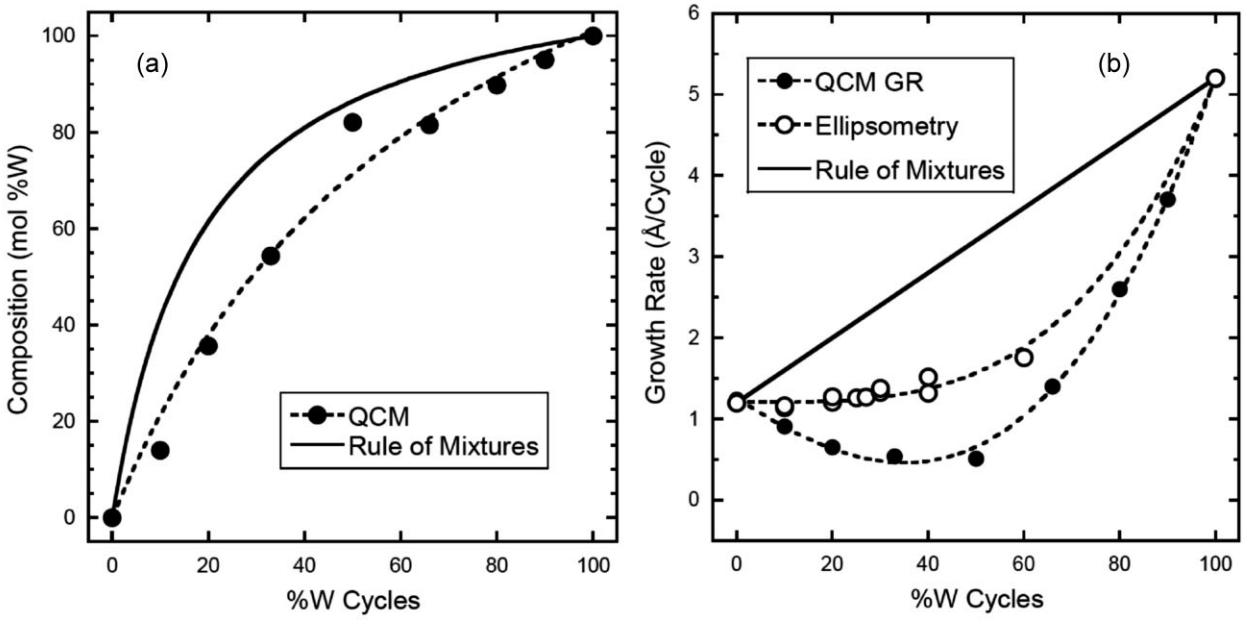

Fig. 3. Composition (a) and growth per cycle (b) of W:Al_2O_3 composite films versus W cycle ratio. Solid circles indicate QCM measurements and open circles show the growth per cycle measured by ellipsometry for W:Al_2O_3 composite films deposited on Si. The solid lines show the rule-of-mixture predictions for the composition and growth per cycle, while the dashed lines are intended to guide the eye.

increase compared to the subsequent cycles. For instance, only 9 ng cm^{-2} is deposited during the TMA/H_2O cycles in the 50% W films compared to the steady-state value of 35 ng cm^{-2} for Al_2O_3 ALD (Fig. 1b). Close inspection of the QCM step structure provides a possible explanation for this behavior. The solid line in Figure 4 shows the QCM mass versus time during the growth of a composite film using 20% W, while the dashed lines denote when the indicated precursors were dosed. The first and third TMA/H_2O cycles in Fig. 4 demonstrate the expected step shape for Al_2O_3 ALD,[41] but the shape for the W cycle and the Al_2O_3 cycle that immediately follows are peculiar. In particular, the Si_2H_6 exposure has no apparent effect on the mass, and the mass change from the TMA exposure following the WF_6 exposure is much smaller than expected for Al_2O_3 ALD. We know from XPS that the films contain fluorine (Section 2.2). Moreover, previous studies demonstrated that alternating exposures to niobium pentafluoride (NbF_5) and TMA produced films comprised of NbF_x, NbC, C, and AlF_3.[39] Consequently, we hypothesize that the first TMA exposure following WF_6 in Fig. 4 might result in:

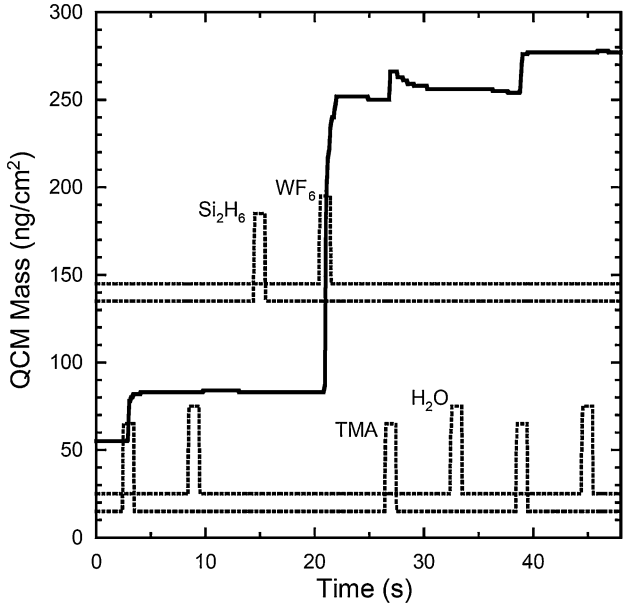

Fig. 4. In situ QCM measurements recorded during the ALD of W:Al_2O_3 composite film using 20% W. Solid line shows the QCM data while dashed lines designate when the indicated ALD precursors were dosed.

$$WF_5^* + Al(CH_3)_3 \rightarrow AlF_3^* + WC^* + 2C^* + 2\,HF + 7/2\,H_2 \quad (1)$$

where the asterisks denote surface species. The net mass change for this process is only 25 amu compared to 56 amu for TMA reacting on an Al_2O_3 surface. Furthermore, the free energy change for the analogous reaction between TMA and WF_6 is -173 kcal mol^{-1} at 200°C indicating thermodynamic favorability.[45] Reaction 1 is highly speculative, but it is consistent with the results from our study and with reference.[39] Detailed in situ measurements of the W:Al_2O_3 composite film ALD are underway in our laboratory, including studies of alternative precursor orderings, to better understand the surface chemistry.

2.2. Characterization of Films

A series of ALD W:Al_2O_3 composite films were prepared on Si substrates using 30% W with varying numbers of ALD cycles. The thicknesses for these films determined by ellipsometry are plotted in Figure 5. Linear least-square analysis (solid line in Fig. 5) yields an excellent fit with a growth per cycle of 1.33Å per cycle indicating that the W:Al_2O_3 composite film thickness can be controlled precisely as expected for an ALD process. To examine the composition and microstructure of the ALD W:Al_2O_3 composite films, a sample was prepared on Si using 500 ALD cycles of W:Al_2O_3 composite with 30% W followed by 50 ALD Al_2O_3 cycles. XPS depth profiling was performed on this sample and the results are shown in Figure 6a. After removing a contamination layer rich in adventitious carbon, the overall elemental composition of the W:Al_2O_3 composite layer is uniform across the film thickness. The XPS depth profiling measurements yielded a sample thickness of 650 Å in fair agreement with the thickness of 725Å determined by spectroscopic ellipsometry.

Fig. 6a shows that the composite layer is composed of O, Al, F, W, and C. Based on the surface chemistries for the ALD Al_2O_3 and ALD W in the composite layers, the presence of F and C is unexpected and likely originates from the unique chemistry that occurs upon transitioning between the W and Al_2O_3 ALD process. As noted above, alternating cycles of niobium NbF_5 and TMA yield films comprised of NbF_x, NbC, C, and AlF_3.[39] The W 4f spectral region (Fig. 6b) shows peaks at 31.8 and 33.8 eV characteristic of metallic W and only a weak shoulder at ~37 eV indicating minimal WO_x.[46–48] From this we conclude that the W is mostly metallic in the composite films.

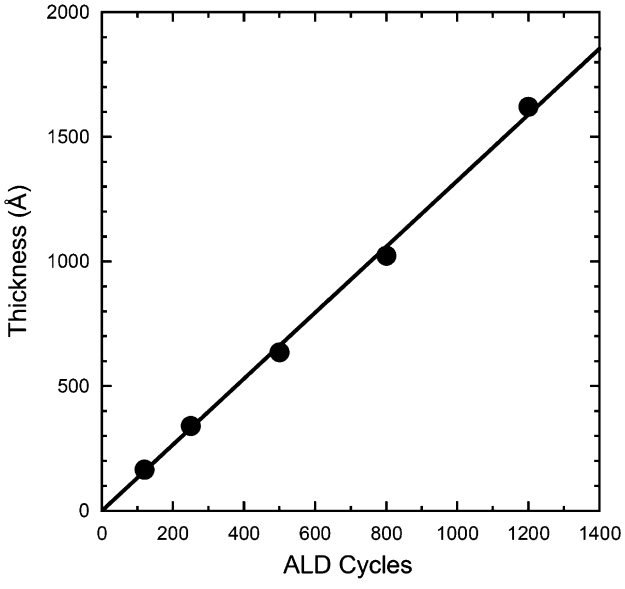

Fig. 5. Thickness versus number of ALD cycles for ALD W:Al_2O_3 composite films deposited on Si substrates using 30% W, as determined by spectroscopic ellipsometry.

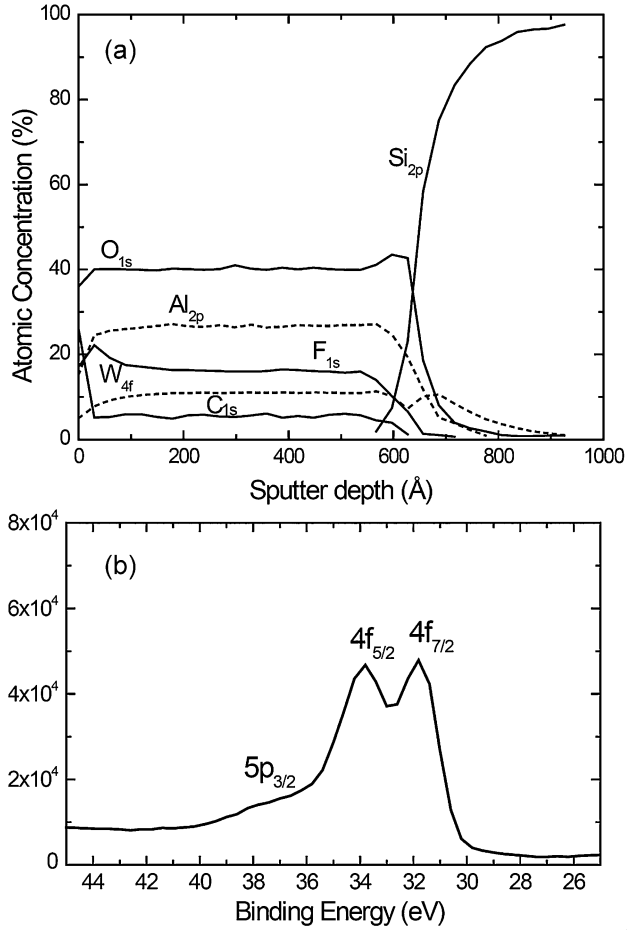

Fig. 6. XPS measurements of ALD W:Al_2O_3 composite film deposited using 500 ALD cycles on Si substrates with 30% W followed by 50 ALD Al_2O_3 cycles. a) Depth profiling measurements showing Al, O, C, and F in the W:Al_2O_3 composite film. b) XPS scan through W 4f spectral region showing peaks at 31.8 and 33.8 eV characteristic of metallic W.

Next, the microstructure of the W:Al_2O_3 composite film with 30% W was evaluated using cross-sectional transmission electron microscopy (TEM). As seen in Figure 7a, the film appears dense and continuous and the top surface is relatively smooth and parallel to the Si substrate surface. Fig. 7b shows a higher resolution TEM image including the substrate-film interface. The interface between the Si substrate and the W:Al_2O_3 composite film shows an amorphous region attributed to the Si native oxide and the initial Al_2O_3 ALD cycles. More importantly, Fig. 7b shows that the W:Al_2O_3 composite film is comprised of 1–2 nm particles (dark spots) embedded in a lower density matrix. Close inspection of the particles reveals weak lattice fringes. Moreover, nanobeam diffraction measurements acquired from the composite film region (not shown) exhibit diffuse rings consistent with crystalline nanoparticles. Based on the XPS measurements, we hypothesize that the crystalline nanoparticles in Fig. 7b are metallic tungsten. These tungsten nanoparticles might form through the sintering of W atoms upon reduction of WF_x surface species

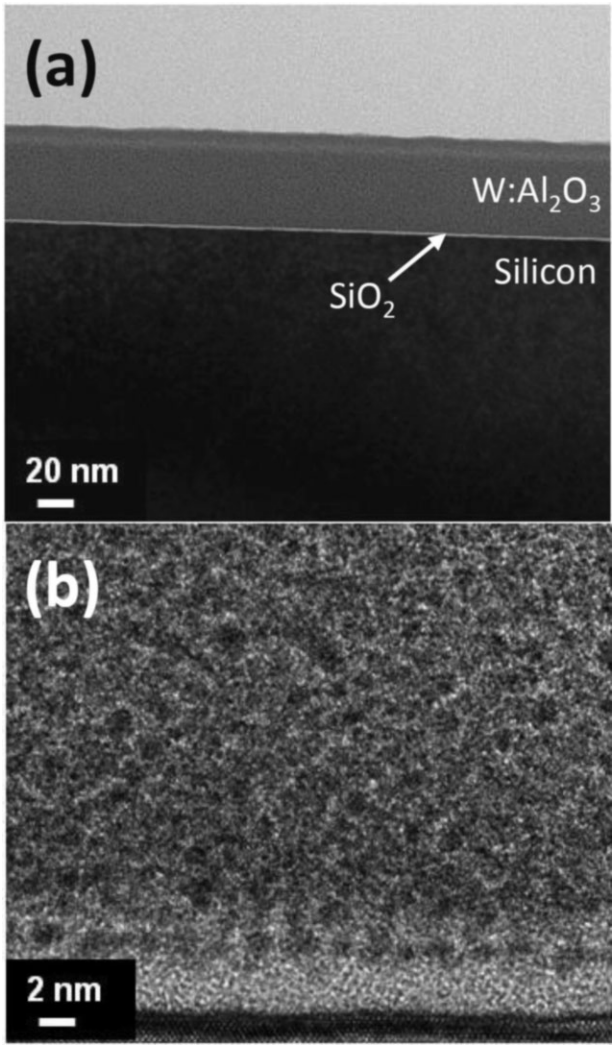

Fig. 7. Cross-sectional TEM image of ALD W:Al_2O_3 composite film deposited on Si substrates with 30% W. a) Low resolution image showing Si substrate and composite film; b) higher resolution image showing nanocrystals embedded in amorphous matrix.

by the TMA. The role of TMA as a reducing agent is unexpected, but we believe this to be true for the following reasons: 1) The microstructure and properties of the W:Al_2O_3 composite films are practically identical with and without the Si_2H_6; and 2) in situ infrared (IR) measurements reveal an increase in the broadband IR absorbance (i.e., the conductivity) of the W:Al_2O_3 composite films when TMA follows a WF_6 exposure. We will elaborate on these findings in a future publication focusing on the mechanism for the W:Al_2O_3 composite film ALD.

2.3. Electrical Resistivity

A series of ALD W:Al_2O_3 composite films was prepared on comb chips and capillary glass arrays with various %W values using 500 ALD cycles and the sheet resistance was determined using current-voltage measurements. Using the film thicknesses determined from spectroscopic ellipsometry, and the known geometry of the capillary glass arrays, the resistivity was calculated and these values are plotted in Figure 8. A wide span of resistivity was observed ranging from $\sim10^{12}$ at 10% W to $\sim10^{8}$ at 30% W with the resistivity decreasing approximately exponentially with increasing %W cycles as demonstrated by the solid line in Fig. 8 showing an exponential decay fit to the data. The resistivity values deduced from the comb chips (solid circles) and capillary glass arrays (open circles) are in good agreement demonstrating that the thickness and composition of the ALD W:Al_2O_3 composite films are uniform in the high aspect ratio (60:1) capillary pores.

The exponential relationship between resistivity and % W cycles shown in Fig. 8 can be rationalized based on the microstructure of the composite films. The TEM and XPS measurements revealed that the composite films are comprised of metallic W nanoparticles embedded in an insulating Al_2O_3 (and AlF_3) matrix. If the conductivity depends on tunneling between the W nanoparticle sheets, then the linear relationship between ALD Al_2O_3 cycles and W nanoparticle sheet spacing would generate the exponential behavior in Fig. 8. Additional studies are underway to elucidate the transport mechanism in these ALD W:Al_2O_3 composite films.

We observed that the ALD W:Al_2O_3 composite film resistivity was nearly constant over a broad range of fields from 10^{4}–$10^{8}\,V\,m^{-1}$, consistent with Ohmic behavior. Furthermore, no breakdown was observed for any of the films even at the highest fields of $10^{8}\,V\,m^{-1}$. These qualities,

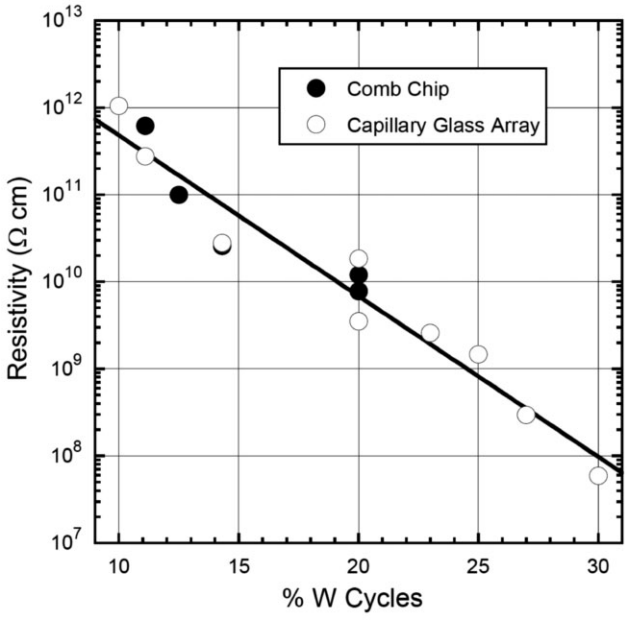

Fig. 8. Resistivity of ALD W:Al_2O_3 composites as a function of % W for films deposited on comb chips (solid circles) and capillary glass arrays (open circles). Solid line shows exponential fit to the resistivity data.

combined with the ability to tune the resistivity over a broad range as shown in Fig. 8, and the capability to coat high aspect ratio substrates, make the ALD W:Al_2O_3 composite films excellent candidates to serve as tunable resistance coatings in electron amplifying devices such as MCPs. In future publications we will elaborate on the synthesis, characterization, and testing of MCPs prepared using these W:Al_2O_3 composite films.

3. Conclusions

Nanocomposite tungsten-aluminum oxide (W:Al_2O_3) thin films with tunable resistivity were prepared by ALD. We first investigated the growth of these materials using in situ QCM measurements to study the effect of the W cycle ratio on the growth per cycle and the W content of the films. These measurements revealed that the W ALD inhibits the Al_2O_3 ALD and vice versa. Next, W:Al_2O_3 composite films were deposited on Si substrates and evaluated using spectroscopic ellipsometry, and these measurements agreed fairly well with the in situ QCM measurements. Depth profiling XPS showed that the films were uniform in composition and comprised of Al, O, and W as expected, but also included F and C. These finding, when combined with the QCM measurements, suggest that the TMA reduces the adsorbed WF_x species to form AlF_3 and metallic W. We intend to follow this initial paper with more detailed studies aimed at achieving a better understanding of the mechanism of W:Al_2O_3 ALD. Cross-sectional TEM revealed that the composite films consist of metal nanoparticles embedded in an amorphous matrix. The resistivity of these composite films can be tuned in the range of $10^{12} - 10^{8}$ Ω cm by adjusting the W cycle ratio between 10 and 30% W. These ALD films have application as functional coatings in electron multipliers and as charge drain coatings on insulating components in electron and ion optics.

4. Experimental

The W, Al_2O_3, and W:Al_2O_3 composite depositions were carried out at 200°C in a hot walled viscous flow ALD reactor described previously.[41] This reactor was equipped with a QCM that facilitated in-situ studies of the ALD processes. The TMA (97%, Aldrich), deionized H_2O, Si_2H_6 (99.998%, Aldrich) and WF_6 (99.8%, Aldrich) precursors were maintained at room temperature. The ultrahigh purity N_2 carrier gas flow was set to 300 sccm, which provided a base pressure of 1.0 Torr in the ALD reaction chamber as measured by a heated Baratron pressure gauge (MKS model 629B). The W:Al_2O_3 composite films were deposited on n-type Si(100) substrates. Prior to ALD, the substrates were cleaned using a 10 min ultrasonic treatment in acetone. For the Al_2O_3 ALD, the precursors TMA and H_2O were alternately pulsed in the continuously flowing N_2 carrier flow with the timing sequence: 1 s TMA dose-5 s N_2 purge-1 s H_2O dose-5 s N_2 purge. The TMA and H_2O partial pressures during the dosing were 0.2 Torr and 0.3 Torr, respectively. Similarly, the W ALD used alternating exposures to WF_6 and Si_2H_6 with the timing sequence: 1 s Si_2H_6 dose-5 s N_2 purge-1 s WF_6 dose-5 s N_2 purge, with partial pressures of 0.25 Torr and 0.05 Torr for the Si_2H_6 and WF_6, respectively. These conditions for the Al_2O_3 and W ALD provided self-limiting growth as verified by in situ QCM measurements.

An in situ QCM study was performed to examine the W:Al_2O_3 composite ALD using different ALD cycle ratios. The QCM measurements typically used longer N_2 purge times of 10 s to allow the QCM signal to stabilize after each precursor exposure. The thicknesses of W:Al_2O_3 layers on Si were determined by ex situ spectroscopic ellipsometry using a Cauchy model (Alpha-SE, J. A. Woollam Co.). TEM analysis was performed by Evans Analytical Group (EAG, Sunnyvale, CA). TEM samples were prepared using the in situ FIB lift out technique on an FEI Strata Dual Beam FIB/SEM. The samples were capped with a protective layer of carbon prior to FIB milling. The samples were imaged with a FEI Tecnai TF-20 FEG/TEM operated at 200kV in bright-field (BF) TEM mode, high-resolution (HR) TEM mode, and nanobeam diffraction (NBD) mode. The composition of the W:Al_2O_3 composite layers was determined by depth profiling XPS (Evans Analytical Group). The relative W content in the W:Al_2O_3 composite films was determined using XRF (Oxford ED2000).

The resistance of the W:Al_2O_3 layers was determined by performing current-voltage (*I–V*) measurements using a Keithley Model 6487 current-voltage source. To facilitate *I–V* measurements on these highly resistive coatings, the films were deposited on insulating substrates with lithographically patterned comb structures comprised of interdigitated Au electrodes with a 2μm spacing. These comb structures provided an effective contact area of 80000 squares, and an equivalent boost in current compared to a conventional four-point probe measurements.[42] Additional *I–V* measurements were performed on W:Al_2O_3 layers deposited on high aspect ratio (60:1) borosilicate glass capillary arrays with 20 μm pores fabricated by Incom, Inc. (Charlton, MA). These capillary arrays were coated on both sides with 100 nm evaporated Ni-Cr to provide a low resistance electrical contact. These substrates were used to evaluate the suitability of the W:Al_2O_3 composite ALD process for MCP fabrication.

Received: January 21, 2013
Revised: April 4, 2013

[1] D. R. Beaulieu, D. Gorelikov, R. de Rouffignac, K. Saadatmand, K. Stenton, N. Sullivan, A. S. Tremsin, *Nucl. Instrum. Methods Phys. Res, Sect. A* **2009**, *607*, 81.

[2] O. H. W. Siegmund, K. Fujiwara, R. Hemphill, S. R. Jelinsky, J. B. McPhate, A. S. Tremsin, J. V. Vallerga, H. J. Frisch, J. Elam, A. Mane, D. C. Bennis, C. A. Craven, M. A. Deterando, J. R. Escolas, M. J. Minot, J. M. Renaud, *Proc. SPIE* **2011**, *8145*, 81450J.

[3] A. U. Mane, Q. Peng, M. J. Wetstein, R. G. Wagner, H. J. Frisch, O. H. W. Siegmund, M. J. Minot, B. W. Adams, M. C. Chollet, J. W. Elam, *Proc. SPIE* **2011**, *8031*, 80312H.

[4] M. Y. Song, Y. Seo, Y. S. Kim, H. D. Kim, H. M. An, B. H. Park, Y. M. Sung, T. G. Kim, *Appl. Phys. Express* **2012**, *5*, 091202.

[5] S. Z. Rahaman, S. Maikap, T. C. Tien, H. Y. Lee, W. S. Chen, F. T. Chen, M. J. Kao, M. J. Tsai, *Nanoscale Res. Lett.* **2012**, *7*, 345.

[6] C. N. Peng, C. W. Wang, J. S. Huang, W. Y. Chang, W. W. Wu, Y. L. Chueh, *J. Nanosci. Nanotechnol.* **2012**, *12*, 6271.

[7] C. C. Lin, Y. P. Chang, *J. Nanosci. Nanotechnol.* **2012**, *12*, 2437.

[8] D. Jana, S. Maikap, T. C. Tien, H. Y. Lee, W. S. Chen, F. T. Chen, M. J. Kao, M. J. Tsai, *Jpn. J. Appl. Phys.* **2012**, *51*, 04DD17.

[9] C. G. Kuo, C. Y. Chou, Y. C. Tung, J. H. Chen, *J. Mar. Sci. Technol.* **2012**, *20*, 365.

[10] A. Maier, B. Tieke, *J. Phys. Chem. B* **2012**, *116*, 925.

[11] Y. S. Lin, J. Y. Lai, *Jpn. J. Appl. Phys.* **2012**, *51*, 01AC03.

[12] D. N. Qu, H. F. Cheng, Y. J. Zhou, X. Xing, D. Q. Liu, *Appl. Mech. Mater.* **2012**, *152–154*, 519.

[13] G. Bodurov, T. Ivanova, M. Aleksandrova, K. A. Gesheva, *J. Phys. Conf. Ser.* **2012**, *356*, 012016.

[14] C. E. Patil, P. R. Jadhav, N. L. Tarwal, H. P. Deshmukh, M. M. Karanjkar, P. S. Patil, *Mater. Chem. Phys.* **2011**, *126*, 711.

[15] J. M. O. R. de Leon, D. R. Acosta, U. Pal, L. Castaneda, *Electrochim. Acta* **2011**, *56*, 2599.

[16] I. Jouanny, S. Labdi, P. Aubert, C. Buscema, O. Maciejak, M. H. Berger, V. Guipont, M. Jeandin, *Thin Solid Films* **2010**, *518*, 3212.

[17] S. Popescu, I. Demetrescu, A. N. Gleizes, *Rev. Chim. -Bucharest* **2007**, *58*, 880.

[18] W. Kulisch, *Nato Sci. Ser. II* **2006**, *223*, 493.

[19] R. Freed, T. Gubiotti, J. Sun, F. Kidwingira, J. S. Yang, U. Ummethala, L. C. Hale, J. J. Hench, S. Kojima, W. D. Mieher, C. F. Bevis, S. J. Lin, W. C. Wang, *Proc. SPIE* **2012**, *8323*, 83230H.

[20] M. A. McCord, P. Petric, U. Ummethala, A. Carroll, S. Kojima, L. Grella, S. Shriyan, C. T. Rettner, C. F. Bevis, *Proc. SPIE* **2012**, *8323*, 832311.

[21] P. Petric, C. Bevis, M. McCord, A. Carroll, A. Brodie, U. Ummethala, L. Grella, A. Cheung, R. Freed, *J. Vac. Sci. Technol. B* **2010**, *28*, C6c6.

[22] P. Petric, C. Bevis, A. Brodie, A. Carroll, A. Cheung, L. Grella, M. McCord, H. Percy, K. Standiford, M. Zywno, *Proc. SPIE* **2009**, *7271*, 727107.

[23] P. Petric, C. Bevis, A. Carroll, H. Percy, M. Zywno, K. Standiford, A. Brodie, N. Bareket, L. Grella, *J. Vac. Sci. Technol. B* **2009**, *27*, 161.

[24] S. M. George, *Chem. Rev.* **2010**, *110*, 111.

[25] J. W. Klaus, S. J. Ferro, S. M. George, *Thin Solid Films* **2000**, *360*, 145.

[26] A. W. Ott, J. W. Klaus, J. M. Johnson, S. M. George, *Thin Solid Films* **1997**, *292*, 135.

[27] R. M. Costescu, D. G. Cahill, F. H. Fabreguette, Z. A. Sechrist, S. M. George, *Science* **2004**, *303*, 989.

[28] F. H. Fabreguette, R. A. Wind, S. M. George, *Appl. Phys. Lett.* **2006**, *88*, 013116.

[29] F. H. Fabreguette, S. M. George, *Thin Solid Films* **2007**, *515*, 7177.

[30] J. W. Elam, S. M. George, *Chem. Mater.* **2003**, *15*, 1020.

[31] J. W. Elam, D. Routkevitch, S. M. George, *J. Electrochem. Soc.* **2003**, *150*, G339.

[32] S. Duenas, H. Castan, H. Garcia, J. Barbolla, K. Kukli, J. Aarik, M. Ritala, M. Leskela, *2005 Spanish Conference on Electron Devices, Proceedings* **2005**, *29*.

[33] J. R. Maldonado, F. Pease, C. J. Hitzman, A. D. Brodie, P. Petric, C. Bevis, M. McCord, W. M. Tong, F. Kidwingira, P. Pianetta, M. Bibee, A. Mehta, R. Bhatia, *J. Vac. Sci. Technol. B* **2011**, *29*, 06F317.

[34] Large-Area Psec Photo-Detectors, https://psec.uchicago.edu/blogs/lappd/ (accessed May, 2013).

[35] M. D. Groner, J. W. Elam, F. H. Fabreguette, S. M. George, *Thin Solid Films* **2002**, *413*, 186.

[36] J. W. Elam, C. E. Nelson, R. K. Grubbs, S. M. George, *Surf. Sci.* **2001**, *479*, 121.

[37] F. H. Fabreguette, Z. A. Sechrist, J. W. Elam, S. M. George, *Thin Solid Films* **2005**, *488*, 103.

[38] A. Rahtu, T. Alaranta, M. Ritala, *Langmuir* **2001**, *17*, 6506.

[39] J. A. Klug, T. Proslier, J. W. Elam, R. E. Cook, J. M. Hiller, H. Claus, N. G. Becker, M. J. Pellin, *J. Phys. Chem. C* **2011**, *115*, 25063.

[40] R. K. Grubbs, C. E. Nelson, N. J. Steinmetz, S. M. George, *Thin Solid Films* **2004**, *467*, 16.

[41] J. W. Elam, M. D. Groner, S. M. George, *Rev. Sci. Instrum.* **2002**, *73*, 2981.

[42] A. Brodie, P. De Cecco, C. Bevis, J. R. Maldonado, B. Ritwik, E. Deguns, G. Sundaram, *ECS Trans.* **2010**, *33*, 101.

[43] M. D. Groner, F. H. Fabreguette, J. W. Elam, S. M. George, *Chem. Mater.* **2004**, *16*, 639.

[44] R. W. Wind, F. H. Fabreguette, Z. A. Sechrist, S. M. George, *J. Appl. Phys.* **2009**, *105*, 074309.

[45] HSC Chemistry 6.1, Outokumpu Research Oy: Pori, Finland **2007**.

[46] A. Katrib, F. Hemming, L. Hilaire, P. Wehrer, G. Maire, *J. Electron Spectrosc. Relat. Phenom.* **1994**, *68*, 589.

[47] O. Y. Khyzhun, *J. Alloy Compd.* **2000**, *305*, 1.

[48] J. F. Moulder, W. F. Stickle, P. E. Sobol, K. D. Bomben, *Handbook of X-ray Photoelectron Spectroscopy, Perkin-Elmer Corp, Eden Prairie* **1992**.

